ARASHI SCIENTIFIC PUBLISHERS

Arashi Journal of Metals & Material Sciences
Volume 1, Issue 1 (Jul-Dec) 2024, pp. 40–46
DOI: 10.54646/jmms.2024.0006
www.asp-jmms.com

SHORT COMMUNICATION

Assembly of Au^+ over deprotonated graphene oxide and its antibacterial activity: A molecular dynamics investigation

Felsis Angelene Daison[1] and Pandian Sokkar[2]*

[1]Faculty of Allied Health Sciences, Chettinad Academy of Research and Education, Kelambakkam, Tamilnadu, India
[2]School of Chemistry, Madurai Kamaraj University, Madurai, Tamil Nadu, India

***Correspondence:**
Pandian Sokkar,
pandian.sokkar@gmail.com

Received: 08 November 2024; **Accepted:** 25 January 2025; **Published:** 08 February 2025

சுருக்கம்:
பாதோஜெனிக் பாக்டீரியாக்கள், ஆண்டிபயாட்டிக்குகளுக்கு எதிர்ப்புத் தன்மையைக் கொண்டிருப்பது சிகிச்சை முறையில் முக்கிய சவால்களை ஏற்படுத்துகிறது. சமீபத்தில், கிராபீன் அடிப்படையிலான நானோதுகள்கள் இத்தகைய எதிர்ப்பு கொண்ட வகைகளுக்கு சிறந்த பாக்டீரிய எதிர்ப்பு செயல்பாட்டைக் காண்பிக்கின்றன, குறிப்பாக தங்கம் (Au) அலங்கரிக்கப்பட்ட கிராபீன் ஆக்சைடு (GO) நானோதுகள்கள். இருப்பினும், அதன் பாக்டீரிய எதிர்ப்பு செயல்திறன் எப்படி செயல்படுகிறது என்பதற்கான அறிவியல் ஆதாரம் சரியாக புரிந்துகொள்ளப்படவில்லை மற்றும் கூடுதல் ஆராய்ச்சி தேவை. அணுஅளவிலான பௌதீக நிகழ்வுகளை ஆராய, மூலக்கூறு இயக்கவியல் (MD) சிமுலேஷன் வழக்கமாக பயன்படுத்தப்படுகிறது, இது எதிர்ப்பு நடத்தையின் நுட்பமான செயல்முறையைப் புரிந்துகொள்ள உதவுகிறது. இங்கு, நீர்ச் சூழலில் ஹைட்ரஜன் அயன்களை இழந்த GO (GO^-) மற்றும் Au^+ அயன்கள் ஒன்றிணையும் முறை MD சிமுலேஷன் மூலம் ஆய்வு செய்யப்படுகிறது. அதனை தொடர்ந்து, மாதிரி பாக்டீரியா மென்பிரேனுடன் GO^-/Au^+ கூட்டத்தின் பாக்டீரிய எதிர்ப்பு செயல்திறனை ஆராயப்பட்டுள்ளது. முடிவுகள், Au^+ அயன்கள் பாஸ்பேட் தலை குழுவுடன் சேரும்போது, பாக்டீரியா மென்பிரேனில் பெரிய துளை உருவாக்கத்தை உணர்த்துகின்றன. GO^-/Au^+ கூட்டத்தின் செயல்பாடு, பாஸ்பேட் தலை குழுவின் திசையை இரட்டை அடுக்கு படலத்தின் ஹைட்ரோபோபிக் உள்புறத்தை நோக்கி மாற்றுகிறது, மேலும் நீர் மூலக்கூறுகளின் இயக்கத்துடன் இணைந்து மென்பிரேனின் ஒருமைப்பாட்டை சீர்குலைக்கிறது. உருவாக்கப்பட்ட துளை குறைந்தது 100 நானோசெக்கன்கள் நிலையாக இருக்கிறது, மேலும் கணிக்கப்பட்ட ΔGperm மதிப்பு -340 kJ/mol ஆகும். எங்கள் ஆய்வு, GO^-/Au^+-ன் பாக்டீரிய எதிர்ப்பு செயல்திறனுக்கான செயல்முறையை மேலும் ஆதரிக்கிறது, இது புதிய வகை பாக்டீரிய எதிர்ப்பு முகவர்களை உருவாக்க உதவக்கூடும்.

Abstract:
Pathogenic bacteria which are resistant to antibiotics pose significant challenges in the treatment procedure. Recently, graphene-based nanoparticles (NPs) are found to display excellent antibacterial activity against such resistant strains, especially gold (Au)-decorated graphene oxide (GO) NPs. However, the mechanistic study behind its antibacterial activity is not understood and needs further research. Molecular dynamics (MD) simulation is routinely employed to investigate physical phenomena at the atomistic level, offering insights into the detailed mechanism behind the resistant behavior. Here, MD simulations are performed to investigate the assembly of deprotonated GO (GO^-) and the Au ions (Au^+) in an aqueous environment, and subsequently, the antibacterial activity of the GO^-/Au^+ assembly with a model bacterial membrane. The results indicate the formation of a large pore in the bacterial membrane, induced by the activity of Au^+ to the phosphate head group. The activity of GO^-/Au^+ changes the orientation of the phosphate head group towards the hydrophobic interior of the bilayer, coupled with the flow of water molecules, ultimately disrupting the membrane integrity. The formed pore is stable for at least 100 ns with a calculated ΔG_{perm} value of -340 kJ/mol. Our study provides further support to the mechanism of the antibacterial activity of GO^-/Au^+, which could help in the development of newer class of antibacterial agents.

Keywords: graphene oxide, gold ions, nanoparticles, antibacterial activity, molecular dynamics simulation, mechanism

Introduction

Nanoparticles (NPs) have recently gained popularity in biomedical and pharmaceutical applications. Many potential applications have been proposed that take advantage of the unique properties of NPs, including drug, gene, and macromolecule delivery vehicles (1–3); hyperthermia and photothermal treatments for cancer therapies (4, 5); and bioimaging (6, 7). Several nanoscale antimicrobial elements, including Ag, AgO, TiO_2, CuO, ZnO, Au, and MgO, have notable broad-spectrum antipathogenic activity (8–16). Carbon-based NPs, including fullerenes and carbon nanotubes with their unique chemical, optical, and mechanical properties, effectively restricted bacterial proliferation when employed as membrane or film substrates, inhibiting microbial growth (17). Meanwhile, it has been confirmed that NPs can disrupt cell membranes and elevate cell death significantly (18). Graphene, graphene oxide (GO), and graphene derivatives have been extensively investigated as anticancer (19), antimicrobial (20), and anti-Alzheimer's disease (21) biological agents or platforms for pharmaceutical conveyance (22). Several approaches have been explored that aim to illustrate the prospective capabilities of these carbon NPs. For instance, in 2010 the first account of the antibacterial activity of GO and reduced GO (rGO) nanosheets was put forth, wherein it was identified that graphene-based NPs were found to be useful in inhibiting *E. coli* growth (23). It was also discovered that by coming into direct contact with bacteria, graphene and GO nanowalls might negatively impact the bacterial cell membrane. In recent years, attention towards compounds derived from graphene has heightened as prospective short-term hindrances of the multiplication of bacterial cells (24, 25). The various influences on the antimicrobial activity of graphene NPs involve NPs properties like electronic and surface chemical characteristics as well as size and other consequential factors along with interacting circumstances such as duration of incubation, concentration, medium, and additional external conditions (26–30). Many studies have shown that physical interactions between the cell walls of bacteria and GO nanosheets may trigger membrane disruptions caused by piercing the pointy edges of thin GO nanosheets (31). Local perturbations like these affect the membrane potential of bacterial cells' lipid bilayers, disrupt cellular metabolism, and eventually damage the cell membrane, resulting in bacterial cell lysis and death (32, 33). The negative impact of graphene on the cell membrane can also be driven by the transfer of charge interaction caused by the direct interaction of the bacterial membrane with graphene, which works as a receiver of electrons in direct exposure to bacteria (34). In the last few years, the antibacterial activity of Au NPs has been investigated (35, 36). Au NPs can cause pores in the bacterial cell wall, allowing cell contents to leak, and they can bind to DNA, preventing transcription. They may also produce oxidative stress through free radical formation: the interaction between small NPs and bacteria most likely causes an imbalance in metabolic processes in the bacterial cell, causing a rise in ROS production and bacterial death (37). Au NPs were further combined with the GO (38). These nanocomposites have greater antimicrobial properties than the individual components, and the disruption of the bacterial cell membrane appears to be caused by the leak of sugars and proteins from the bacterial cell membrane when it encounters the nanocomposite (38). In this study, GO is improved by attaching Au^+ ions on the outer layer of GO nanosheets through an *in-silico* route, which guarantees 2 benefits: increasing antibacterial activity through the synergistic effect of Au^+ ions and GO (39). However, the molecular mechanism of this nanocomposite acting on the bacterial cell membrane remains unknown. To the best of our knowledge, the effect of Au^+ ions with GO on a bacterial cell membrane in an external electric field has not been studied. Using an atomistic molecular dynamics (MD) simulation, the activity of Au^+ ions conjugated with a GO membrane on a bacterial cell membrane in the presence of an external electric field is examined in this study.

Materials and methods

Models of nanoparticle

GO decorated with epoxy and hydroxyl groups was used for the modeling studies. The outermost edges of GO were derivatized by carboxyl groups in the deprotonated state to be consistent with the ionization of GO at a pH of 7.4. The modeled GO had a molecular weight of 1600 Da.

MD simulation

Lipid components were simulated using the CHARMM36 force field in conjunction with the TIP3P water model. Force field parameters for molecules 1 and 2 were generated using the CGENFF36 force field. These parameters were automatically determined through the ParamChem service integrated within the CHARMM-GUI web platform (40). MD simulations were executed employing the GROMACS-4.5.3 software (41). All simulations were conducted within the isothermal-isobaric ensemble, maintaining a pressure of 1 atm and a temperature of 310 K. The Parrinelo-Rahman barostat and V-rescale thermostat were employed for pressure and temperature control, respectively (42). Integration of the equation of motion was achieved using a discrete time step of 2 femtoseconds (fs). The calculation of electrostatic interactions employed the Particle Mesh Ewald summation method with a non-bonded cutoff distance of 10 Å (43). Hydrogen-heavy atom bonds were harmonically

constrained at their equilibrium lengths using the linear constraint solver (LINCS) algorithm (44).

Initial phases of the study encompassed energy minimization and subsequent equilibration of the systems for a duration of 200 picoseconds (ps). Subsequently, production runs spanning 100 nanoseconds (ns) were carried out across all systems. Introduction of 0.15 M sodium chloride (NaCl) was added to match the physiological conditions. Trajectories were stored at intervals of 10 ps for subsequent analyses. The GROMACS suite of programs and Visual Molecular Dynamics (VMD) software were employed for trajectory analysis (45).

To comprehend the conformational and structural alterations induced by nanomaterials (NMs) within the membrane, it is imperative to acknowledge the influence of the selected force field on the study outcomes. Data obtained from the 3 distinct simulations were subjected to meticulous analysis to attain statistical significance.

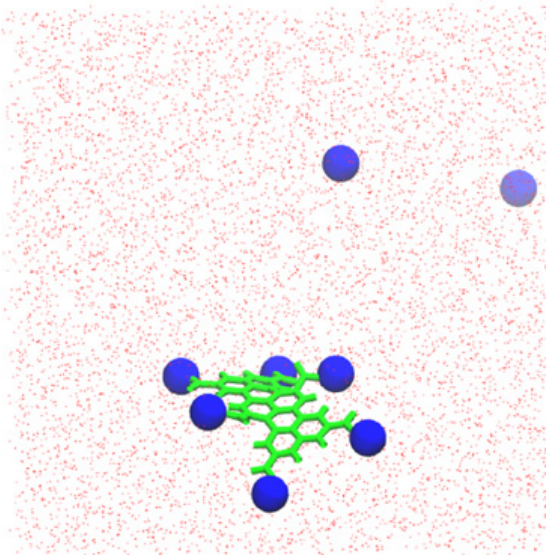

FIGURE 1 | Snapshot of Au^+ ions binding with GO^- simulation. Color code: The red dots were water molecules, green dots were GO^-, and blue dots were Au^+ ions.

Free energy analysis

To calculate the potential of mean force (PMF) for pore formation, the reaction coordinate was defined as the distance between a positively charged center of the GO^- and Au^+ ions compound and the bilayer's center along the z-axis (membrane normal). Two "pull groups" were established: the positively charged center and the entire lipid bilayer.

A harmonic force constant of 1000 kJ/mol·nm^2 and a pulling rate of 0.0001 nm/ps were applied to pull these groups towards each other along the z-axis. This process generated 22 windows between 0.0 nm and 2.1 nm, with a step size of 0.1 nm. Each window was sampled for 20 ns while applying a restraining force constant of 3000 kJ/mol·nm^2 to explore the conformational space around the fixed reaction coordinate. The GROMACS "pull code" was used to restrain the distance between the groups along the reaction coordinate. Finally, the PMF was extracted from the data using the Weighted Histogram Analysis Method (WHAM) (46) tool in GROMACS.

Data analysis

The data underwent analysis from numerous sets of trajectories within each system, ensuring the attainment of a conclusion with statistical significance.

Results and discussion

MD simulations

MD simulation has become a crucial aspect of molecular interpretation. The simulation model has simplified the condition of experimental techniques by revealing the molecular mechanisms at the atomic level. With this *in-silico* method, we embarked on a process of enhancing deprotonated GO (GO^-) with Au^+ ions, which we then subjected to testing against bacterial membranes. Our approach involved running simulations to confirm the binding between GO^- and Au^+ ions within an aqueous environment (**Figure 1**). These simulations spanned approximately 100 ns to ensure comprehensive evaluation. The introduced Au^+ ions bound with GO^- sheets perfectly.

Subsequently, we employed the configuration where Au^+ ions were bound to the GO^- (GO^-/Au^+) and introduced it into a bacterial-mimicking membrane environment. To gain a comprehensive understanding of the antibacterial mechanisms inherent to GO^-/Au^+, we formulated 2 distinct models, one with 8 molecules of GO^-/Au^+ and the other with 6 molecules of GO^-/Au^+. The GO^-/Au^+ were strategically positioned vertically above the phospholipid bilayer comprised of anionic DMPG (1,2-Dimyristoyl-sn-glycero-3-phosphoglycerol) and zwitterionic DMPC (1,2-Dimyristoyl-sn-glycero-3-phosphocholine) molecules (**Figure 2**).

We initially verified that in this setup, the GO^-/Au^+ molecules disrupt the lipid bilayer but the desired pore was not formed in the given 100 ns simulation (**Figure 3**). This configuration enabled the visualization of potential interactions between GO^-/Au^+ and the lipid bilayers. The GO^-/Au^+ sheets were not able to disrupt the bacterial cell membrane. These models were devised to investigate the interaction between GO^-/Au^+ with a bilayer membrane made up of DMPG as well as DMPC. The simulations were executed within the canonical ensemble NVT (fixed amount of substance (N), volume (V), and temperature

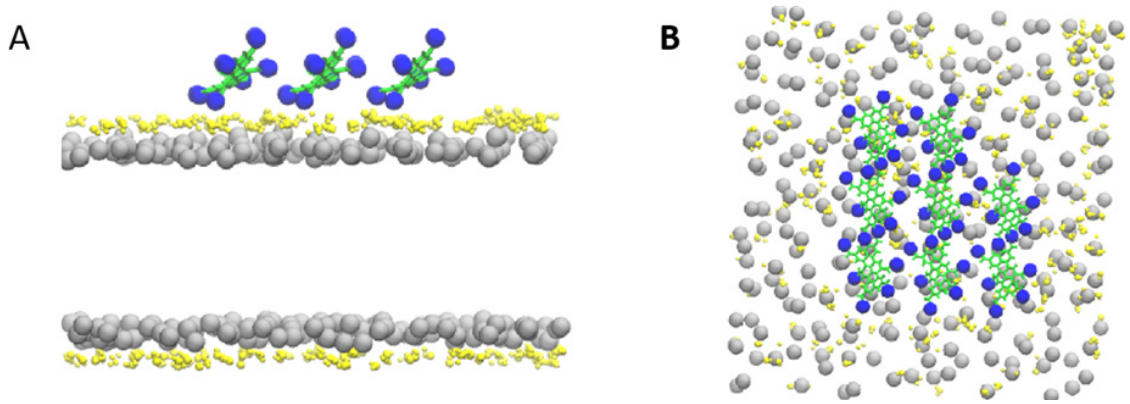

FIGURE 2 | Snapshots of the initial configuration of GO^{-} with Au^{+} ions. **(A)** Side view. **(B)** Upper view. Color code: yellow dots were water molecules, gray dots were lipid bilayers, green dots were GO^{-}, and blue dots were Au^{+} ions.

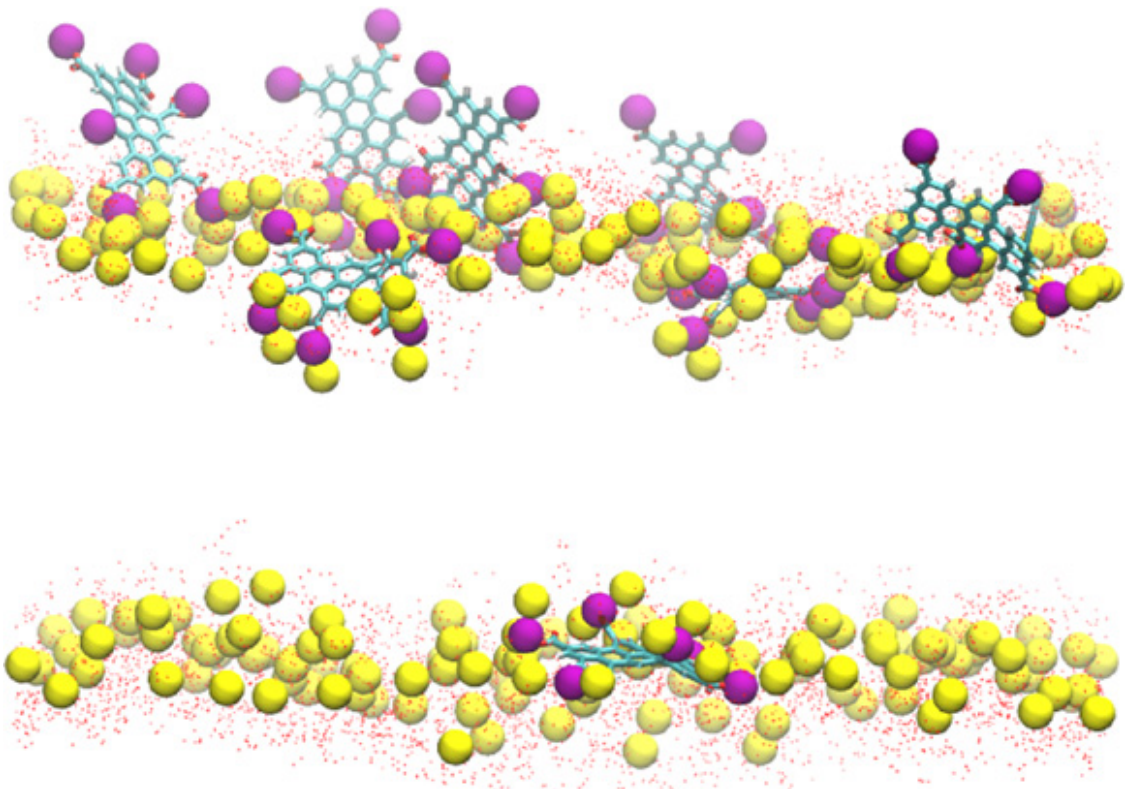

FIGURE 3 | Snapshots of simulation with 8 molecules of GO^{-}/Au^{+}. Color code: red dots were water molecules, yellow dots were lipid bilayers, blue dots were GO^{-}, and magenta were Au^{+} ions.

(T)), employing a time step of 1 fs over a duration of 300 ps to achieve equilibrium within the system. Additional MD simulations were subsequently conducted, employing a time step of 1 fs over 100 ps, to facilitate further analysis. Consequently, snapshots capturing the initial and final states of the GO^{-}/Au^{+} models were generated because of these MD simulations. Importantly, the MD simulations revealed a substantial reconfiguration of the GO-Au composite upon its interaction with the phospholipid bilayer.

Consecutively, 8 molecules of GO^{-}/Au^{+} were placed inside the lipid bilayer and simulation was executed. During this simulation, which ran for around 100 ns, we observed that within the initial 10 ns, the complex induced the creation of a substantial pore within the bacterial membrane. This was accomplished by disrupting the phosphate groups present in the bilayer. The GO^{-}/Au^{+} exhibited the ability to draw the phosphate head groups from the bilayer's exterior into its interior, alongside water molecules. This concerted movement resulted in the formation of the pore. This disruptive process led to the establishment of a stable pore structure that endured throughout the simulation period. As the GO^{-}/Au^{+} proceeded towards the interior of the bilayer,

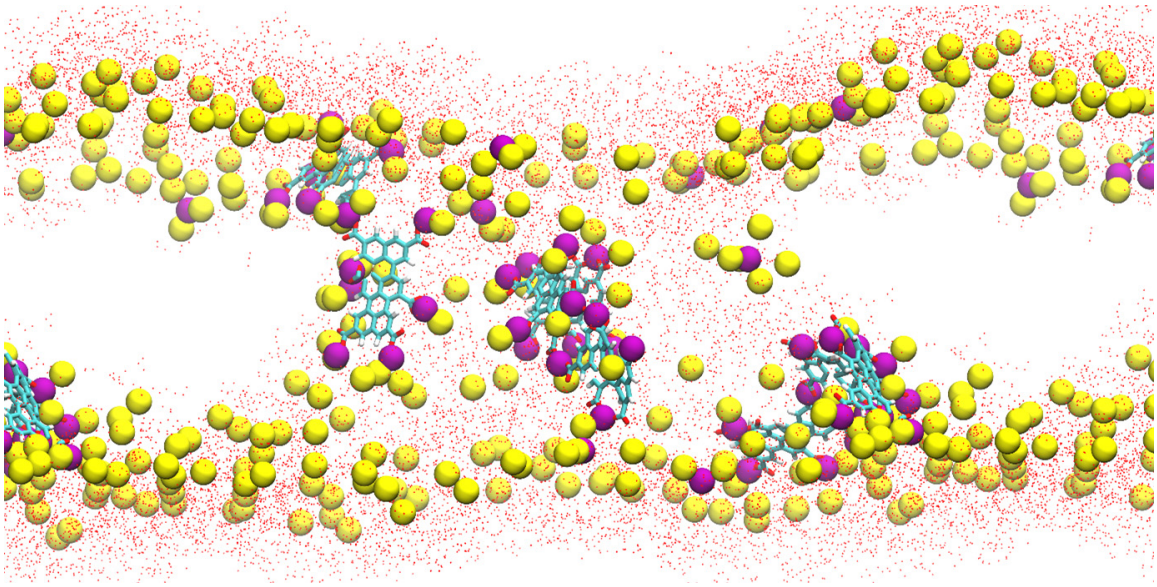

FIGURE 4 | Snapshots of simulation with 8 molecules of GO^{-}/Au^{+}. Color code: red dots were water molecules, yellow dots were lipid bilayers, blue sheets were GO^{-}, and magenta dots were Au^{+} ions.

it engendered the formation of this pore, subsequently giving rise to regions on the bilayer surface that lacked lipid head groups. This, in turn, altered the texture of the bilayer surface (**Figure 4**). Given that the phospholipid bilayer serves as a fundamental component of cellular membranes, functioning as a protective barrier regulating the internal concentrations of ions, proteins, and molecules, the disruption caused by GO^{-}/Au^{+} molecules warranted an in-depth exploration of their prospective antimicrobial activity. This clearly proves that the GO^{-}/Au^{+} have antibacterial activity, and the mechanism of the activity is through membrane damage.

The GO^{-} nanosheets possess substantial π-conjugated structures with marked hydrophobic characteristics, facilitating interactions with phospholipid molecules within cellular membranes through hydrophobic forces. Consequently, the viability of microorganisms can be influenced by such interactions. The extraction of lipid tails from the cellular membrane, induced by the GO^{-}/Au^{+} system, accelerates nanoscale dewetting of water. This phenomenon is expedited through hydrophobic interactions, as the phospholipids extensively cover the entire surface of GO^{-}/Au^{+} molecules, thereby maximizing contact. This process was further strengthened by the positive charge of the Au^{+} ions that were conjugated to GO^{-} sheets.

Considering these observations, MD simulations conducted utilizing atom-based force fields have proven instrumental in elucidating the molecular mechanisms underlying the alteration of bacterial cell membrane integrity by forming a pore induced by GO^{-}/Au^{+} system. This analytical approach aids in identifying the intricate processes through which GO^{-}/Au^{+} molecules can impact the structural integrity of bacterial cell membranes.

Free energy analysis

Our initial step involved generating the free energy profile to analyze the interactions between GO^{-}/Au^{+} and the membrane. This allowed us to gain insights into the thermodynamics of the system and understand the preferences of the GO^{-}/Au^{+} with respect to the bilayers. Subsequently, we computed the PMF of the GO^{-}/Au^{+} by considering their z-distance from the center of the bilayer. This calculation provided valuable information about the energy landscape of the system. We calculated the PMF for the bilayer normal translation of GO^{-}/Au^{+} compound using umbrella sampling and WHAM analysis. The reaction coordinate was defined as the distance between the positively charged center and the bilayer center. The PMF profiles showed a free energy barrier for membrane permeation (ΔGperm), with the maximum at the bilayer center and the minimum near the bilayer-water interface.

The calculated ΔGperm values for GO^{-}/Au^{+} were −340 kJ/mol (**Figure 5**). This compound formed pores, and their ΔGperm values corresponded to the pore formation free energy.

Despite the expectation that highly active compounds should have a lower ΔGperm our calculations showed the opposite. This discrepancy might be attributed to the higher energy cost associated with burying the +2 formal charge of the compound. The molecular interactions stabilizing the pore structure were insufficient to offset this energy cost.

It's important to note that our calculations did not consider cooperative effects arising from multiple compounds. These cooperative effects are complex to model and hinder the investigation of structure-activity relationships for pore-forming antimicrobials. Consequently, rational design of

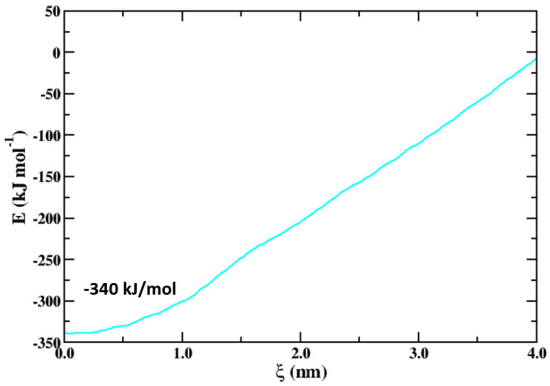

FIGURE 5 | Snapshots of free energy for membrane permeation constructed by umbrella sampling. The distance between the bilayer center and the positive charge center was used as the reaction coordinate.

such compounds remains challenging. Additionally, we attempted to identify parameters that could serve as metrics for pore-forming ability but encountered limitations.

Conclusion

This study provides compelling evidence for the potent antibacterial activity of GO^-/Au^+ molecules. Our MD simulations reveal a novel mechanism of action whereby these nanostructures induce the formation of stable pores in bacterial membranes. The binding of Au^+ to phosphate head groups, coupled with the hydrophobic interactions of GO^-, disrupts the lipid bilayer integrity, leading to membrane permeabilization. Our findings underscore the potential of GO^-/Au^+ molecules as promising candidates for the development of novel antimicrobial agents. In comparison to conventional antimicrobial therapies, such as antibiotics and metal-based treatments, GO^-/Au^+ nanomaterials offer several potential advantages. First, their ability to induce membrane disruption via a dual mechanism of electrostatic and hydrophobic interactions could reduce the likelihood of resistance development, a major concern with traditional antibiotics. Moreover, the use of gold (Au^+) ions may contribute to enhanced biocompatibility and stability, improving the overall therapeutic profile. However, unlike antibiotics that target specific bacterial pathways, the broad mechanism of action of GO^-/Au^+ nanomaterials may present challenges in specificity, potentially affecting beneficial bacteria or human cells. Despite their promising antimicrobial properties, several limitations must be considered. One of the key challenges with GO^-/Au^+ composites is the risk of toxicity due to the oxidative properties of Au^+ and GO^-. Further investigations into their biocompatibility, particularly *in-vivo*, will be essential to assess any potential side effects.

Future studies should focus on testing the efficacy of GO^-/Au^+ composites against a wider variety of clinically relevant bacterial strains, including antibiotic-resistant pathogens. This would establish whether the observed antibacterial activity is broadly applicable or strain-specific. Also exploring practical applications, such as the incorporation of GO^-/Au^+ nanostructures into antimicrobial coatings for medical devices or wound dressings, could be a promising direction. Additionally, formulating these nanomaterials into stable suspensions or controlled-release systems could improve their therapeutic efficiency and application in clinical settings.

References

1. Wilczewska A, Niemirowicz K, Markiewicz K, Car H. Nanoparticles as drug delivery systems. *Pharmacol Rep.* (2012) 64:1020–37.
2. Rana S, Bajaj A, Mout R, Rotello V. Monolayer coated gold nanoparticles for delivery applications. *Adv Drug Deliv Rev.* (2012) 64:200–16.
3. Shao K, Singha S, Clemente-Casares X, Tsai S, Yang Y, Santamaria P. Nanoparticle-based immunotherapy for cancer. *ACS Nano.* (2015) 9:16–30.
4. Perigo E, Hemery G, Sandre O, Ortega D, Garaio E, Plazaola F, et al. Fundamentals and advances in magnetic hyperthermia. *Appl Phys Rev.* (2015) 2:041302.
5. Jaque D, Maestro L, del Rosal B, Haro-Gonzalez P, Benayas A, Plaza J, et al. Nanoparticles for photothermal therapies. *Nanoscale.* (2014) 6:9494–530.
6. Mieszawska A, Mulder W, Fayad Z, Cormode D. Multifunctional gold nanoparticles for diagnosis and therapy of disease. *Mol Pharm.* (2013) 10:831–47.
7. Bogart L, Pourroy G, Murphy C, Puntes V, Pellegrino T, Rosenblum D, et al. Nanoparticles for imaging, sensing, and therapeutic intervention. *ACS Nano.* (2014) 8:3107–22.
8. Azam A, Ahmed A, Oves M, Khan M, Habib S, Memic A. Antimicrobial activity of metal oxide nanoparticles against Gram-positive and Gram-negative bacteria: a comparative study. *Int J Nanomed.* (2012) 7:6003–9.
9. Besinis A, De Peralta T, Handy R. The antibacterial effects of silver, titanium dioxide and silica dioxide nanoparticles compared to the dental disinfectant chlorhexidine on *Streptococcus mutans* using a suite of bioassays. *Nanotoxicology.* (2014) 8:1–16.
10. Emami-Karvani Z, Chehrazi P. Antibacterial activity of ZnO nanoparticle on gram-positive and gram-negative bacteria. *Afr J Microbiol Res.* (2011) 5:1368–73.
11. Usman M, Zowalaty M, Shameli K, Zainuddin N, Salama M, Ibrahim NA. Synthesis, characterization, and antimicrobial properties of copper nanoparticles. *Int J Nanomed.* (2013) 8:4467–79.
12. Lyon D, Fortner J, Sayes C, Colvin V, Hughes J. Bacterial cell association and antimicrobial activity of a C60 water suspension. *Environ Toxicol Chem Int J.* (2005) 24:2757–62.
13. Kang S, Mauter M, Elimelech M. Physicochemical determinants of multiwalled carbon nanotube bacterial cytotoxicity. *Environ Sci Technol.* (2008) 42:7528–34.
14. Zhu Z, Meng H, Liu W, Liu X, Gong J, Qiu X, et al. Superstructures and SERS properties of gold nanocrystals with different shapes. *Angewandte Chemie Int Edn.* (2011) 50:1593–6.
15. Li Z, Cheng E, Huang W, Zhang T, Yang Z, Liu D, et al. Improving the yield of mono-DNA-functionalized gold nanoparticles through dual steric hindrance. *J Am Chem Soc.* (2011) 133:15284–7.
16. Xia Y, Nguyen T, Yang M, Lee B, Santos A, Podsiadlo P, et al. Self-assembly of self-limiting monodisperse supraparticles from polydisperse nanoparticles. *Nat Nanotechnol.* (2011) 6:580–7.

17. Deryabin D, Efremova LV, Vasilchenko A, Saidakova EV, Sizova E, Troshin P, et al. A zeta potential value determines the aggregate's size of penta-substituted [60] fullerene derivatives in aqueous suspension whereas positive charge is required for toxicity against bacterial cells. *J Nanobiotechnology.* (2015) 13:1–13.
18. Pietroiusti A. Health implications of engineered nanomaterials. *Nanoscale.* (2012) 4:1231–47.
19. Lim D, Sim M, Oh L, Lim K, Park H. Carbon-based drug delivery carriers for cancer therapy. *Arch Pharm Res.* (2014) 37:43–52.
20. Martynková G, Valášková M. Antimicrobial nanocomposites based on natural modified materials: a review of carbons and clays. *J Nanosci Nanotechnol.* (2014) 14:673–93.
21. Li J, Han Q, Wang X, Yu N, Yang L, Yang R, et al. Reduced aggregation and cytotoxicity of amyloid peptides by graphene oxide/gold nanocomposites prepared by pulsed laser ablation in water. *Small.* (2014) 10:4386–94.
22. Liu J, Cui L, Losic D. Graphene and graphene oxide as new nanocarriers for drug delivery applications. *Acta Biomater.* (2013) 9:9243–57.
23. Hu W, Peng C, Luo W, Lv M, Li X, Li D, et al. Graphene-based antibacterial paper. *ACS Nano.* (2010) 4:4317–23.
24. Perreault F, De Faria A, Elimelech M. Environmental applications of graphene-based nanomaterials. *Chem Soc Rev.* (2015) 44:5861–96.
25. Akhavan O, Ghaderi E. Toxicity of graphene and graphene oxide nanowalls against bacteria. *ACS Nano.* (2010) 4:5731–6.
26. Li Y, Yuan H, von Dem Bussche A, Creighton M, Hurt RH, Kane AB, et al. Graphene microsheets enter cells through spontaneous membrane penetration at edge asperities and corner sites. *Proc Natl Acad Sci.* (2013) 110:12295–300.
27. Mao J, Guo R, Yan L. Simulation and analysis of cellular internalization pathways and membrane perturbation for graphene nanosheets. *Biomaterials.* (2014) 35:6069–77.
28. Yin H, Tang H, Wang D, Gao Y, Tang Z. Facile synthesis of surfactant-free Au cluster/graphene hybrids for high-performance oxygen reduction reaction. *ACS Nano.* (2012) 6:8288–97.
29. Zhao S, Li Y, Yin H, Liu Z, Luan E, Zhao F, et al. Three-dimensional graphene/Pt nanoparticle composites as freestanding anode for enhancing performance of microbial fuel cells. *Sci Adv.* (2015) 1:e1500372.
30. Li Y, Tang J, He L, Liu Y, Liu Y, Chen C, et al. Core–shell upconversion nanoparticle@ metal–organic framework nanoprobes for luminescent/magnetic dual-mode targeted imaging. *Adv Mater.* (2015) 27:4075–80.
31. Chen J, Peng H, Wang X, Shao F, Yuan Z, Han H. Graphene oxide exhibits broad-spectrum antimicrobial activity against bacterial phytopathogens and fungal conidia by intertwining and membrane perturbation. *Nanoscale.* (2014) 6:1879–89.
32. Liu S, Zeng T, Hofmann M, Burcombe E, Wei J, Jiang R, et al. Antibacterial activity of graphite, graphite oxide, graphene oxide, and reduced graphene oxide: membrane and oxidative stress. *ACS Nano.* (2011) 5:6971–80.
33. Gurunathan S, Han J, Dayem A, Eppakayala V, Kim J. Oxidative stress-mediated antibacterial activity of graphene oxide and reduced graphene oxide in *Pseudomonas aeruginosa*. *Int J Nanomed.* (2012):5901–14.
34. Wang Z, Tonderys D, Leggett S, Williams E, Kiani M, Steinberg R, et al. Wrinkled, wavelength-tunable graphene-based surface topographies for directing cell alignment and morphology. *Carbon N Y.* (2016) 97: 14–24.
35. Azam A, Ahmed F, Arshi N, Chaman M, Naqvi A. One step synthesis and characterization of gold nanoparticles and their antibacterial activities against *E. coli* (ATCC 25922 strain). *Int J Theor Appl Sci.* (2009) 1:1–4.
36. Annamalai A, Christina V, Sudha D, Kalpana M, Lakshmi PV. Green synthesis, characterization and antimicrobial activity of Au NPs using *Euphorbia hirta* L. leaf extract. *Colloids Surf B Biointerfaces.* (2013) 108:60–5.
37. Bindhu M, Umadevi M. Antibacterial activities of green synthesized gold nanoparticles. *Mater Lett.* (2014) 120:122–5.
38. Hussain N, Gogoi A, Sarma R, Sharma P, Barras A, Boukherroub R, et al. Reduced graphene oxide nanosheets decorated with Au nanoparticles as an effective bactericide: investigation of biocompatibility and leakage of sugars and proteins. *Chempluschem.* (2014) 79:1774–84.
39. Zheng K, Li K, Chang T, Xie J, Chen P. Synergistic antimicrobial capability of magnetically oriented graphene oxide conjugated with gold nanoclusters. *Adv Funct Mater.* (2019) 29:1904603.
40. Jo S, Kim T, Iyer V, Im W. CHARMM-GUI: a web-based graphical user interface for CHARMM. *J Comput Chem.* (2008) 29:1859–65.
41. Abraham M, Murtola T, Schulz R, Páll S, Smith J, Hess B, et al. GROMACS: high performance molecular simulations through multi-level parallelism from laptops to supercomputers. *SoftwareX.* (2015) 1–2:19–25.
42. Parrinello M, Rahman A. Polymorphic transitions in single crystals: a new molecular dynamics method. *J Appl Phys.* (1981) 52:7182–90.
43. Essmann U, Perera L, Berkowitz M, Darden T, Lee H, Pedersen LG. A smooth particle mesh Ewald method. *J Chem Phys.* (1995) 103:8577–93.
44. Hess B, Bekker H, Berendsen H, Fraaije JGEM. LINCS: a linear constraint solver for molecular simulations. *J Comput Chem.* (1997) 18:1463–72.
45. Humphrey W, Dalke A, Schulten K. VMD: visual molecular dynamics. *J Mol Graph.* (1996) 14:33–8.
46. Kumar S, Rosenberg J, Bouzida D, Swendsen R, Kollman PA. THE weighted histogram analysis method for free-energy calculations on biomolecules. I. The method. *J Comput Chem.* (1992) 13:1011–21.